Numerical modeling and seismic performance analysis of a large-scale single-layer lattice dome with a three–dimensional hybrid isolation system subjected to near-field ground motions

Huidong Zhang[*1,2], Xinqun Zhu[3], Xiao Liang[1,2], Zhanyuan Gao[1,2]

[1]School of Civil Engineering, Tianjin Chengjian University, Tianjin 300384, PR China

[2]Tianjin Key Laboratory of Civil Buildings Protection and Reinforcement, Tianjin 300384, PR China

[3]School of Civil and Environmental Engineering, University of Technology Sydney, NSW 2007, Australia

Abstract: At present, a large number of studies and applications have been carried out on horizontal seismic isolation systems, and their effectiveness has been indicated. However, it is necessary to consider multidimensional seismic actions, including the vertical seismic component, because of the spatial characteristics of earthquakes, especially for long-span spatial structures, in which the vertical seismic load plays an important role. In this paper, a hybrid system with three–directional seismic isolation effects is presented and investigated, in which the triple friction pendulum component (TFPC) and the viscous damping component (VDC) are combined in series into the hybrid seismic isolation system. Compared with other seismic isolation systems, the advantages of this hybrid seismic isolation system are that it can not only greatly lengthen the structural periods but also dissipate the seismic energy in all three directions. A numerical modeling method for this hybrid seismic isolation bearing is developed using OpenSees. The seismic performance of a welded super large-scale single-layer lattice dome with this hybrid seismic isolation system subjected to seven near-field ground motions is analyzed. The results show that the important dynamic demands (structural displacements and axial forces of members) in the dome are significantly suppressed compared with the base-fixed dome. The seismic isolation effects are also evaluated in all three directions, and the effectiveness of the hybrid isolation system is verified. Finally, a comparative study is performed, and the geometrical and mechanical parameters of this hybrid bearing are also discussed. The proposed seismic isolation system and its numerical modeling method provide an attractive and effective alternative for the design of long-span spatial structures with seismic isolation systems.

Key words: hybrid isolation system; large-scale single-layer lattice dome; numerical modeling; seismic performance; near-field ground motions.

1. Introduction

In the past 30 years, great efforts have been made to improve the structural performance of buildings subjected to earthquake ground motions, and significant achievements have been made. A base (or bearing) isolation system is one of the most popular means of protecting a structure against earthquake forces because it can considerably reduce the earthquake-induced forces in the superstructure [1]. Therefore, in the earthquake prone countries, the strategy of base (or bearing) isolation has been increasingly adopted to mitigate or reduce potential damage caused by earthquake ground motions. Meanwhile, the concept of base isolation has also received increasing academic and professional attention and is being applied to a wide range of civil engineering structures [2].

Many kinds of isolation systems exist or have been proposed by researchers and engineers. The typical isolation system can be obtained by the use of various bearings [3-9] such as low damping rubber bearings (LDRBs), high damping rubber bearings (HDRBs), lead-rubber bearings (LRBs), friction pendulum bearings (FPBs), ball bearings (BBs), and spring bearings (SBs). Because these bearings or other systems provide flexibility at the base of the structure, most of the earthquake-induced dynamic demands are suppressed. In recent years, several new buildings with

isolation devices have utilized rubber (or elastomeric) bearings [10] and friction pendulum bearings [11].

The existing research achievements [12] show that a large number of studies and applications have been conducted on horizontal isolation systems, and the effectiveness of horizontal isolation technologies has been shown. However, these technologies do not prevent vertical seismic forces from being transmitted directly into the superstructure, especially for long-span spatial structure, because of the spatial characteristics of earthquakes. Therefore, the above conventional isolation systems cannot provide effective vertical seismic isolation performance [13]. Furthermore, criticism has been raised by researchers against conventional horizontal isolation systems because of their vulnerability to long-period ground motions that might cause the large lateral displacements of the isolators [8, 9]. These drawbacks have motivated the development of alternative strategies to achieve the effects of three–direction seismic isolation. Therefore, there is considerable interest worldwide in three–directional isolation systems. Some attempts [14-20] have been made to improve isolation performance by (1) using a complete three–dimensional seismic isolation system and (2) combining vertical isolation system with horizontal isolation system into a hybrid seismic isolation system. More recently, Cesmeci and Gordaninejad *et al*. [21] experimentally investigated a three–dimensional seismic isolation system, which combines the various damping mechanisms and liquid spring features in a single unit serving as the vertical component of the isolation system. However, it should be pointed out that it is impossible for a seismic isolation system to provide superior isolation performance under all earthquake ground motions.

Large-scale single-layer lattice domes have been widely considered to be important buildings. Its superior seismic performance is conducive to the safety of people's lives and economic property. Compared with conventional structures, a large-scale single-layer lattice dome is more complex due to its larger span, dense and complex modes, modal coupling effects, and vertical stability. To ensure structural safety, it is necessary to implement reliable seismic protection measures. In recent years, structural vibration control technology has been applied to large-scale single-layer lattice domes [5, 22-26]. However, to the best of our knowledge, only several typical papers [27, 28, 29] have investigated the seismic performance of large-scale single-layer lattice domes (or large-scale space truss structures) with three–dimensional isolation systems subjected to earthquake ground motions. The investigation and development of the three–dimensional isolation systems for large-scale single-layer lattice domes have received more attention from researchers.

On the other hand, near-field ground motions are different from ordinary ground motions. The research on structural damage during earthquakes and related events [30] shows that the near-field ground motions are characterized by intense velocity and long-period displacement pulses due to the directivity effects as well as hanging wall effects, and there is a destructive potential for structures with long periods. When large-scale single-layer lattice domes with flexible isolation systems are subjected to near-field ground motions, they could result in more serious consequences compared with far-field ground motions. Therefore, investigating the seismic performance of structures with flexible isolation systems subjected to near-field ground motions is necessary.

In this study, based on the characteristics of three–dimensional seismic isolation, a hybrid seismic isolation system with three–directional isolation effects is proposed, in which the triple friction pendulum component (TFPC) and the viscous damping component (VDC) are combined in series into a hybrid seismic isolator. A numerical modeling method for this hybrid seismic isolator is developed in OpenSees (Open System for Earthquake Engineering Simulation), and the mechanical behaviors of the

hybrid seismic isolator are analyzed. Then, the hybrid isolation system is applied to a welded super large-scale single-layer lattice dome. The seismic performance of this dome subjected to 7 near-field ground motions is investigated. The seismic isolation effect for the hybrid system is evaluated. Finally, the important design parameters of the hybrid seismic isolation bearing are discussed.

2. A hybrid isolation system

2.1 Description of the hybrid isolation bearing

This hybrid isolation bearing is circular in shape and composed of the viscous damping component and the sliding component in series. It includes the upper viscous damper component (VDC) and the lower triple friction pendulum component (TFPC). The diagram of the circular hybrid isolation bearing is shown in Fig. 1(a).

In the upper VDC, there is a cavity filled with oil. Connected to the superstructure is the piston rod system, which is supported by vertical springs (or helical springs) in the VDC. Therefore, the viscous damper and the springs form a parallel system. The VDC can horizontally move on the spherical concave surface; however, the VDC is considered to be stiff in shear in this paper. The piston rod system can only move vertically in oil, which leads to a vertical damping force due to the viscosity of the oil.

The TFPC has four concave surfaces coated with synthetic materials. The inner slider can slide horizontally along the inner surfaces of the articulated sliders, while the articulated sliders can slide horizontally along the inner surfaces of the top and bottom plates. The TFPC is considered to be stiff in compression and has a very small stiffness in tension.

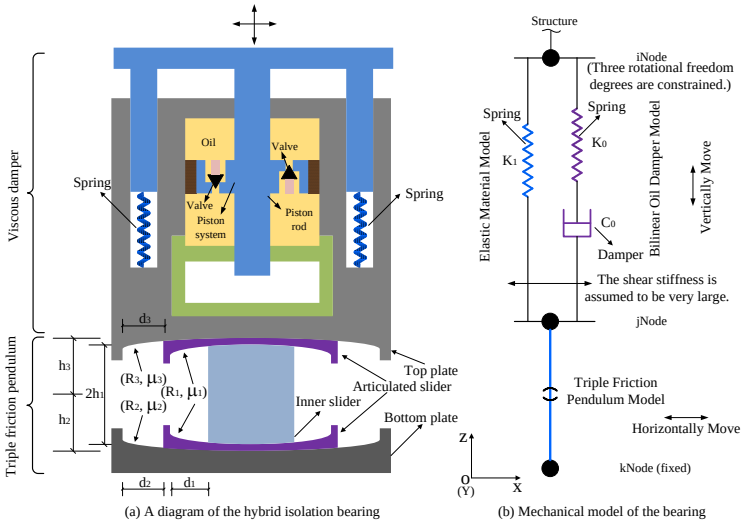

Fig. 1 A hybrid isolation system and its numerical model.

2.2 Properties of the hybrid isolation bearing

In this study, the friction coefficients depending on both the sliding rate and the normal force are considered. To avoid a large lateral sliding distance, the lower inner slider and articulated sliders will be hooked by the bottom and top plates with a very large lateral stiffness when a lateral limit distance d_l that depends on the slip distances d_1, d_2, and d_3 is reached.

Compared with conventional isolation bearings, this hybrid seismic isolation bearing has the following properties and advantages:

- The horizontal sliding behaviors in the TFPC can dissipate more seismic input energy and reduce the negative effects for the superstructure. Compared with the single friction pendulum bearing, the TFPC can produce relatively large displacements and rotations as well as better energy dissipation

capacity. There is no obvious resonance region in the TFPC because of the friction mechanism; therefore, it can retain good energy dissipation ability in a wide frequency band. The smaller friction coefficients of the concave surfaces between the inner slider and the articulated sliders lead to the low horizontal stiffness, which can prolong the structural vibration periods in the horizontal directions and effectively avoid resonance during many earthquakes. In addition, the bearing has a certain degree of self-reset characteristics due to the existence of concave surfaces and boundary limits, which do not lead to a large lateral residual deformation. In the TFPC, large lateral displacements can be limited to avoid structural instability because of the large boundary stiffness.

- In the vertical direction, the springs in the VDC are used for bearing gravity load. The VDC can dissipate the vertical seismic input energy by viscous damping. Compared with the conventional VDCs that can only bear dynamic axial force, the VDC in this paper can also bear the shear force, and its shear stiffness is very large to avoid shear failure horizontally; thus, the horizontal shear energy is dissipated by the TFPC. By choosing the appropriate supporting springs, a vertical flexible region rather than a rigid connection is formed in the VDC, which can lengthen the vertical vibration periods to avoid the vertical resonance.

Because the two components are connected in series, their coupling behaviors can be considered horizontally and vertically together. Therefore, this hybrid isolation bearing is a three–dimensional bearing that can not only prolong the natural vibration periods of a structure but also dissipate the seismic energy in all three directions.

2.3 Modeling method for the hybrid isolation bearing

2.3.1 Triple Friction Pendulum Model

The TFPC is modeled using the *Triple Friction Pendulum Model* [31] in OpenSees. The model is a three–dimensional model with variable friction coefficients [31, 32], and it can account for the vertical-horizontal coupling and the bidirectional coupling in horizontal behavior. In the model, the effects of both the velocity and vertical force on the friction coefficients can be accounted for. The friction coefficients at the slow and fast velocities are obtained based on the following equations [33, 34]:

$$\begin{cases} \mu_s = a_s \times W^{\wedge}(n_s - 1) \\ \mu_f = a_f \times W^{\wedge}(n_f - 1) \\ a_{s,f} = \alpha_0 + \alpha_1 \times W + \alpha_2 \times W^2 \\ \mu = \mu_f - \left(\mu_f - \mu_s\right) \times exp\left(-a_{s,f} \times \dot{u}\right) \end{cases} \tag{1}$$

where a_s, a_f, n_s, and n_f are constants that determine the friction coefficients; μ_s and μ_f are the friction coefficients at the slow and fast velocity, respectively; μ is the friction coefficient; α_0, α_1, and α_2 are the constants; $\dot{u}$ is the velocity at the sliding interface; W is the axial force of the bearing; and $a_{s,f}$ is the constant at slow velocity or fast velocity. Herein, velocities less than 0.02 m/s are characterized as low, whereas velocities greater than 0.25 m/s are characterized as high. The friction characteristics of the triple friction pendulum can be modeled using the *VelNormalFrcDep* friction model in OpenSees. Generally, the sliding friction coefficients of the TFPC range between 0.005 and 0.3 [35].

In the geometry model of the triple friction pendulum, the effective radius of each friction surface is obtained by the expression $L_i = R_i - h_i (i = 1, 2, 3)$. The horizontal limit displacement of the bearing is given by the expression $d_l = 2d_1 + d_2 + d_3 + L_1 \times d_3/L_3 - L_1 \times d_2/L_2$. By limiting the value of d_l, it is possible to ensure that there is no excessive slip in the structure as a whole. There is more

information on this model in the Dao and Ryan et al. [31] study.

2.3.2 Bilinear Oil Damper Model

The VDC is modeled using the *Bilinear Oil Damper Model* [36] in OpenSees. This model simulates the hysteretic response of bilinear oil dampers with relief valves. For the pure viscous component, the force produced by a bilinear oil damper can be computed as follows:

$$F_d(t) = \begin{cases} C_d \dot{u}_d(t), |F_d(t)| \le F_{rf} \\ \mathrm{sgn}(\dot{u}_d(t)) \left(F_{rf} + pC_d \left(|\dot{u}_d(t)| - \dot{u}_{rf}(t) \right) \right), |F_d(t)| > F_{rf} \end{cases} \quad (2)$$

where C_d, $F_d(t)$, and F_{rf} are the damping coefficient, damping force, and relief force, respectively; $\dot{u}_d(t)$ is the dashpot velocity; $\dot{u}_{rf}(t)$ is the relief velocity; and p is the post relief damping coefficient ratio. In addition to the above pure viscous component, a real viscous damper includes several other components, e.g., steel braces, clevises, brackets and gusset plates [36]. These components provide additional axial stiffness K_0 to the damper.

2.3.3 Mechanical behaviors of the hybrid isolation bearing

A numerical model is developed for this hybrid seismic isolation bearing in OpenSees, as shown in Fig. 1(b). In the bearing, the springs are modeled using the *Elastic Material Model*. Here, the springs and the oil damper are in parallel, and the TFPC system and the VDC system are in series. The VDC is modeled using a *twoNodeLink* element, while the TFPC is modeled using the *Triple Friction Pendulum bearing* element. The mechanical behaviors of the hybrid seismic isolation bearing subjected to a three–dimensional earthquake ground motion (Chi-Chi, CHY101, 1999) are investigated using the parameters listed in Tables 1–4. In Table 1, $K_{v,c}$, $K_{v,t}$, and s_d are the assumed compression stiffness, tension stiffness, and stick distance of the friction surfaces, respectively. The parameter values in Table 2 are obtained according to Eq. (1) and the previous study [31]. The results are shown in Fig. 2.

Table 1 TFPC parameters.

Geometry parameter					
L_1 /m	L_2 /m	L_3 /m	d_1 /m	d_2 /m	d_3 /m
0.26	1.1	1.1	0.05	0.1	0.1

Table 2 Friction parameters of the TFPC.

Friction parameters (depending on the velocity and normal force)				
$(\mu_{f,1}, \mu_{s,1})$	$(\mu_{f,2}, \mu_{s,2})$	$(\mu_{f,3}, \mu_{s,3})$	(n_f, n_s)	$(\alpha_0, \alpha_1, \alpha_2)$
(0.02,0.02)	(0.217,0.173)	(0.217, 0.173)	(0.7, 0.8)	(25, 0, 0)

Table 3 Property of the TFP bearings.

Property of the bearings				
$K_{v,c}$	$K_{v,t}$ /(N/m)	s_d /m	d_l /m	W /N
stiff	0	0.001	0.3	1e5

Table 4 VDC parameters.

Property	K_0 /(N/m)	C_0 /(N/(m/s))	p	K_1 /(N/m)	F_{rf} /N
Value	2e7	1e6	0.2	1e7	2.0e4

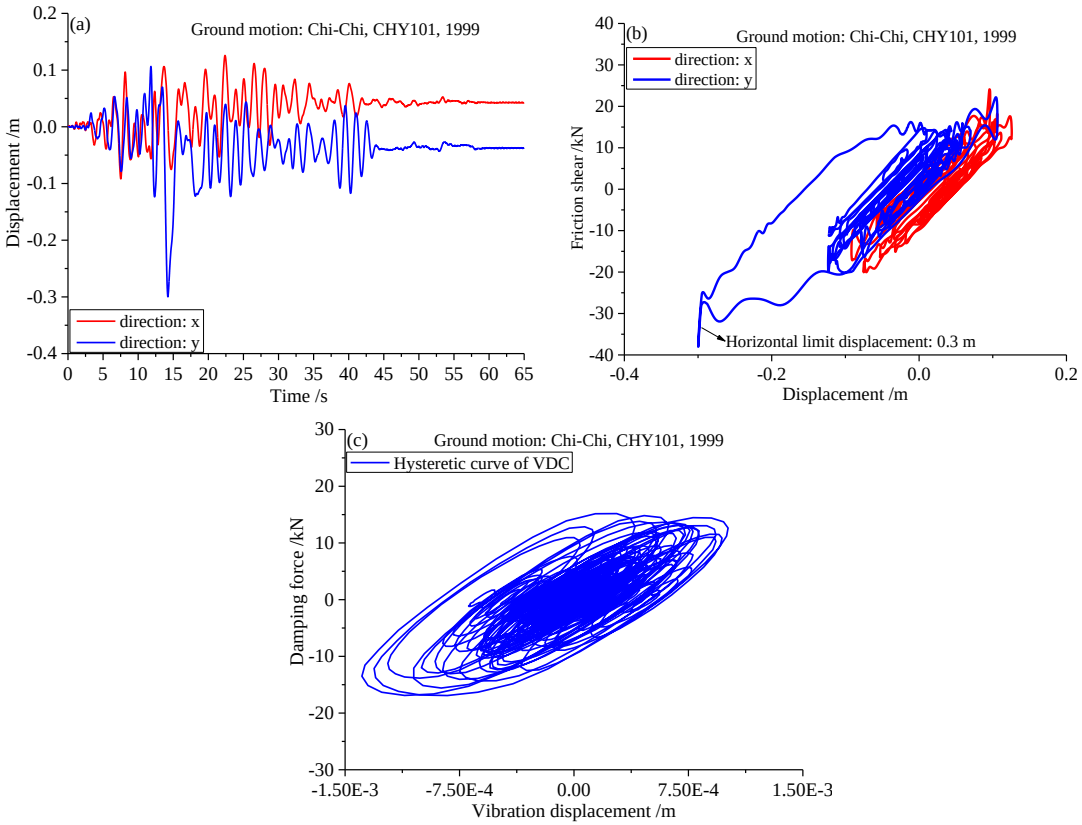

Fig. 2 Mechanical behaviors of the hybrid isolation bearing system under an earthquake.

Fig. 2(a) shows the horizontal slip displacements of the bearing. It is observed that there is an impulse response with a maximum value of 0.3 m in the *y* direction. The lateral limit displacement is 0.3 m according to Table 1, as shown in Fig. 2(b). After the limit displacement is reached, the lateral reaction force of the bearing increases sharply because of the sudden increase of the boundary stiffness, which limits the larger lateral displacement of the bearing. A large lateral displacement in a bearing often has an adverse effect on the stability of a structure. Fig. 2(b) shows that in the hysteresis loops, the shear stiffness is constantly changing during the earthquake, and the shapes of these hysteresis loops are irregular. This occurs because the vertical seismic force is constantly changing, and the shear stiffness and friction force vary with the vertical force in the friction bearing. During the earthquake, the concave surfaces of the friction pendulum slide in turn, and this changes the hysteretic performance of the bearing, showing different shear stiffness and damping characteristics with increasing lateral displacement. Through the reasonable design for the triple friction pendulum, the bearing can have reasonable shear stiffness and damping to meet multiple fortification objectives. Fig. 2(c) shows the hysteresis loops of the VDC. According to the hysteresis loops obtained under the very small vertical deformations, it is found that the VDC presents a good energy dissipation capacity. We define an index ξ_v to describe the equivalent damping characteristic of the VDC. Based on an energy analysis, the index can be approximately evaluated using Eq. (3) [5][37],

$$\begin{cases} \xi_v = \frac{1}{4\pi}\frac{E_d}{N*\bar{E}_s} \\ E_d = \int_{u_1}^{u_2} F_v(u)du \approx \sum_{i=1}^{n-1} F_v\left(\frac{u_i+u_{i+1}}{2}\right)(u_{i+1}-u_i) \end{cases} \tag{3}$$

where E_d, $\bar{E}_s$, and $F_v(u)$ are the energy dissipation, the mean strain energy of the VDC, and the damping force, respectively; N is the number of half cycles; and u_i is the vertical displacement at the i^{th} time step. Here, it is assumed that the mean value of the strain energy peaks is 2 times the mean

strain energy. According to Eq. (3), the damping index ξ_v is as high as 26.8%. Clearly, the VDC presents a good damping performance.

3. Numerical example: A welded super large-scale single-layer lattice dome

3.1 Model details

The structure analyzed in this paper is a welded super large-scale single-layer dome, and its span length and height are 120 m and 27.08 m, respectively, as shown in Fig. 3(a). Its height to span ratio is approximately 1/4.4. The transverse, longitudinal and vertical directions are respectively denoted as axes X, Y and Z in Fig. 3(a). The steel pipes are used as the members of the dome. The internal pipes have an inner radius of 0.09 m and an outer radius of 0.10 m, and their wall thickness is 0.01 m. The inner and outer radii of the outermost steel pipes in the circumferential direction are 0.44 m and 0.5 m, respectively. The elastic modulus, yield stress and mass density of steel material are equal to 2.06×10^{11} Pa, 250 MPa and 7800 kg/m^3, respectively. The strain-hardening ratio of steel material is set to 0.02. The uniform roof load is 150 kg/m^2, and it is assumed to be concentrated at the joints as masses. Some typical positions for outputting dynamic demands are marked in Fig. 3(b).

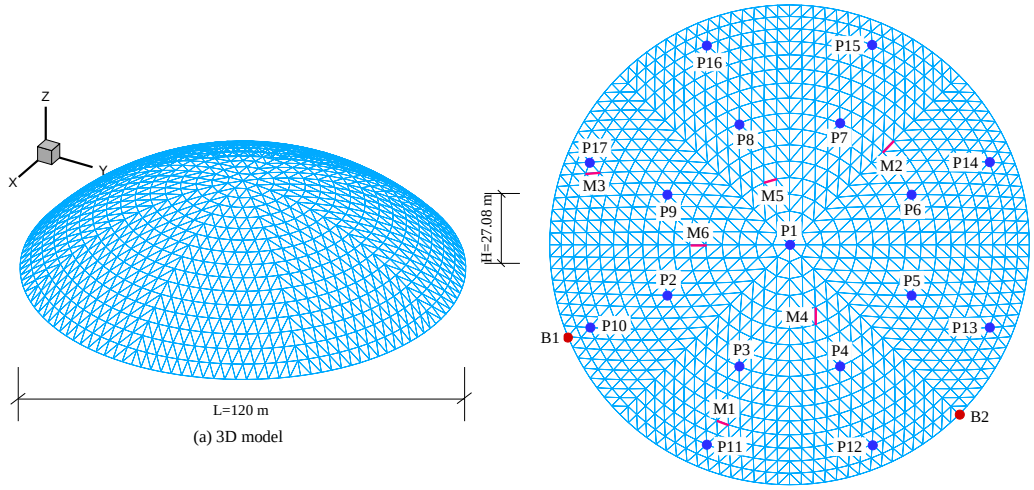

(a) 3D model

(b) plane model

Fig. 3 Dome structure.

3.2 Modeling details

A three–dimensional numerical model for the dome is developed in the OpenSees platform. The single steel member is modeled with a displacement-based nonlinear beam-column element with five integration points along the element length. To trace potential flexural yielding within the cross sections, a *steel02* material model is assigned to the fiber-based cross sections that are assigned to the nonlinear beam-column elements. The fiber discretization of each cross section consists of 20×5 fibers along the circumferential and radial directions. The numerical model consists of 1345 nodes and 3392 elements, including 128 hybrid isolation bearings at supports of the dome. The *P-Delta* transformation is assigned to the steel members of the dome to consider the second–order effects. The viscous damping forces of the structure are modeled with the Rayleigh model (Hall model [38]), in which the current stiffness matrix of the structure and a damping ratio of 2% are adopted for the numerical model. The hybrid isolation bearing is modeled using the developed methods in *Section 2.3* in this paper. Newmark's average acceleration method is used for the nonlinear response history analysis.

3.3 Earthquake ground motions

To consider the effectiveness of the hybrid seismic isolation system and the uncertainties of ground motions, 7 natural near-field seismic records are used for the structural dynamic analysis in this paper.

These seismic records are obtained from the database of the Pacific Earthquake Engineering Research Center (PEER, http://peer.berkeley.edu/). Table 5 summarizes the detailed information of 7 natural seismic records, and Fig. 4 plots the pseudo-acceleration spectra of these natural ground motions. In the spectra, the larger pseudo-acceleration values are mainly in the periods of 0.03 s–1.0 s. The dominant-mode periods of the dome without seismic isolation system fall well within this interval according to an eigenvalue analysis (see *Section 3.4*).

Table 5 Earthquake records for this study.

Earthquake	Year	Recording station	PGA /g			Mw	Duration /s
			x	*y*	*z*		
Imperial Valley	1979	Delta	0.06	0.118	0.021	6.5	18.13
Kobe, Japan	1995	Nishi-Akashi	0.483	0.464	0.387	6.9	40.96
Loma Prieta	1989	Capitola	0.511	0.439	0.556	6.9	40.0
Chi-Chi, Taiwan	1999	CHY101	0.34	0.4	0.166	7.6	65.0
Friuli, Italy	1976	Tolmezzo	0.357	0.315	0.277	6.5	36.39
Northridge	1994	Beverly Hills-14145 Mulhol	0.443	0.488	0.325	6.7	29.99
Manjil, Iran	1990	Abbar	0.514	0.497	0.538	7.4	46.0

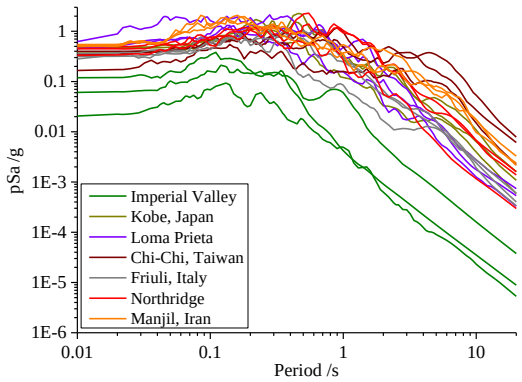

Fig. 4 Pseudo-acceleration spectra of 7 natural seismic records.

3.4 Structural natural vibration properties

After the gravity load is applied to the structure, the natural vibration periods of the dome are obtained based on an eigenvalue analysis. It should be noted that the structural modes associated with friction behaviors are nonlinear. Unlike the conventional linear eigenvalue analysis process, for the structures with the friction-type isolation systems, the gravity must be applied first (that is, the static analysis must be performed first), so that the lateral stiffness of the isolation system can be produced due to the static friction force, and then the eigenvalue analysis is performed. Otherwise, the rigid modes will be obtained.

To avoid the structural periods of the dominant modes (the first several modes) being within the range of 0.03 s to 1.0 s, the parameters of the hybrid isolation bearings are first adjusted to ensure that these periods are greater than 1.0 s. The adjusted important geometrical and mechanical parameters are listed in Table 6. Other parameters are selected from Tables 1–4. Using these parameters, the first 10 modal periods of the original structure (denoted as ″O.S″) and the isolated structure (denoted as ″I.S″) are listed in Table 7, in which the differences between the O.S and I.S are shown.

Table 6 Some parameters of the hybrid isolation bearing.

Parameters of two components						
$(\mu_{f,1},\mu_{s,1})$	$(\mu_{f,2},\mu_{s,2})$	$(\mu_{f,3},\mu_{s,3})$	W /N	K_0 /(N/m)	K_1 /(N/m)	F_{rf} /N
(0.006,0.006)	(0.199,0.161)	(0.199,0.161)	1.2e5	5e6	2.5e5	3.0e4

As expected, the natural vibration periods of the I.S are prolonged, and the periods of the first several modes of the I.S are 3 to 4 times those of the O.S. The first 6 nonlinear modes are shown in Fig. 5. The first three modes of the I.S involve deformations only in the isolation system, while the superstructure is almost ″rigid″. The vertical deformation in the isolation system is predominant for the first mode, whereas the second and third modes are characterized by the horizontal deformations in the isolation system. The other modes involve coupling deformations in both the isolation system and the superstructure. Clearly, the use of the hybrid isolation bearings changes the dynamic characteristics of the original dome. Additionally, in structures with isolation bearings, it is difficult to excite the higher modes during an earthquake.

The prolonging of the dominant-mode periods can lead to smaller spectrum acceleration values in the isolated structures than in the fixed-base structures, thus resulting in smaller structural dynamic demands. This is the most important reason that the isolated structures are protected from damage during an earthquake.

Table 7 Modal periods of the O.S and I.S.

Mode number	Natural vibration period /s		Difference
	O.S	I.S	
1	0.402	1.52	278 %
2	0.402	1.205	199 %
3	0.365	1.205	230 %
4	0.365	0.38	4.1 %
5	0.362	0.38	5.0 %
6	0.362	0.375	3.6 %
7	0.3617	0.375	3.7 %
8	0.3617	0.371	2.6 %
9	0.36	0.371	3.1 %
10	0.36	0.37	2.8 %

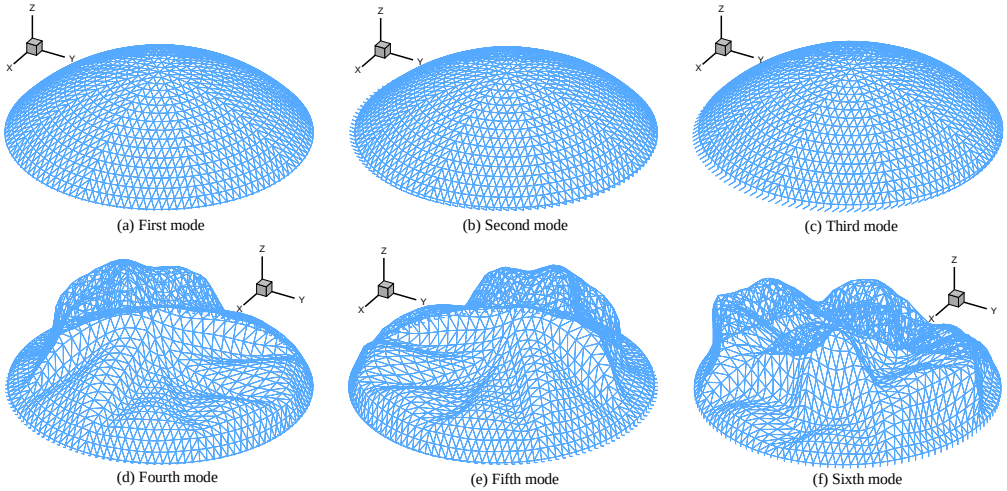

(a) First mode (b) Second mode (c) Third mode

(d) Fourth mode (e) Fifth mode (f) Sixth mode

Fig. 5 Nonlinear modes of the dome.

4. Results

4.1 Structural displacement

Structural displacement is one of the most important dynamic demands for the dome that is subjected mainly to compressive stresses because a large structural displacement can lead to structural instability. Controlling structural displacement is an effective measure for improving structural stability. Using the developed method for the hybrid isolation bearing, the structural displacements are obtained by a dynamic time history analysis. The top of a dome is the typical position, which approximately represents the vibration state of the whole structure.

For comparison, the dynamic time history displacements at P1 (at the top) in the O.S and I.S under three−directional seismic loadings (Kobe, Japan) are shown in Fig. 6. It is observed that compared with the O.S, these dynamic displacements of the I.S are greatly suppressed in all three directions during the earthquake, and the vibrating periods of the responses in the I.S are longer than those in the O.S, indicating that the vibrating velocities decrease. The dynamic responses are well controlled because of the use of the hybrid isolation bearings.

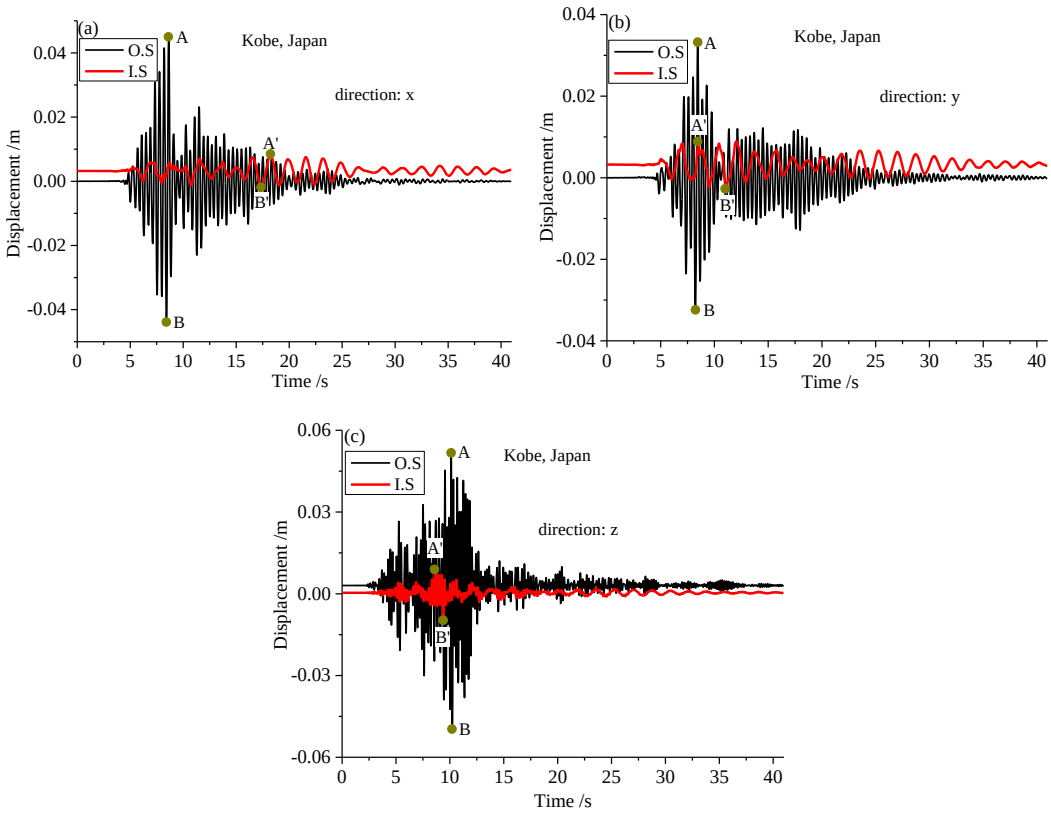

Fig. 6 Dynamic displacements at P1 under an earthquake (Kobe, Japan).

In Fig. 6, the symbols A and B represent the maximum and minimum vibrating displacements at the top of the O.S, respectively; while A' and B' represent the maximum and minimum vibrating displacements at the top of the I.S, respectively. The following parameters are defined as the vibrating amplitudes and the index describing the difference between the O.S and I.S,

$$\begin{cases} u = |u_A - u_B| \\ u' = |u_A{}' - u_B{}'| \\ D_f = {(u - u')}/{u} \end{cases} \tag{4}$$

where u and u' are the nodal vibrating amplitudes of displacements of the O.S and I.S, respectively; D_f is the isolation effect index. If $D_f > 0$, it indicates that the isolation effect is effective; otherwise, it is ineffective, and a higher value means better seismic isolation effect. To further investigate the effect

of isolation bearings on displacement, dynamic analyses under all of the above earthquake conditions are performed. Based on the above analysis method, the vibrating amplitudes and the indexes are listed in Table 8.

Table 8 Dynamic displacements and isolation effect indexes at P1 in the O.S and I.S.

Earthquake	Displacement								
	x /m			*y* /m			*z* /m		
	O.S	I.S	D_f	O.S	I.S	D_f	O.S	I.S	D_f
Imperial Valley	0.0033	3.6e-4	***0.89***	0.0043	8.2e-4	***0.81***	0.002	4.2e-4	***0.79***
Kobe	0.0896	0.009	***0.90***	0.0656	0.011	***0.83***	0.10	0.0176	***0.82***
Loma Prieta	0.077	0.012	***0.84***	0.0612	0.007	***0.89***	0.127	0.0094	***0.93***
Chi-Chi	0.0223	0.01	***0.55***	0.051	0.0183	***0.64***	0.0194	0.0066	***0.66***
Friuli	0.03	0.0056	***0.81***	0.0358	0.0042	***0.88***	0.04	0.0054	***0.87***
Northridge	0.0525	0.011	***0.79***	0.0505	0.0166	***0.67***	0.0817	0.0123	***0.85***
Manjil	0.0472	0.0077	***0.84***	0.0435	0.0129	***0.70***	0.0834	0.0147	***0.82***

As seen from the data listed in Table 8, the use of isolation bearings can effectively suppress the dynamic displacements in all three directions of the dome. Generally, the isolation effect indexes are as high as 0.7–0.9. The isolation effect indexes are 0.5–0.7 only under the Chi-Chi earthquake ground motion; however, in this case, these hybrid bearings also greatly suppress the deformations and improve the stability of the structure. Since the isolation bearings are more flexible than those of the base-fixed structure, most of the lateral and vertical motions occur in the isolation bearings. As a result, the superstructure experiences less deformation. This could potentially lead to less damage in the superstructure.

4.2 Bearing responses

The typical hysteretic curves of the TFPCs under three–directional seismic loadings (Northridge, 1994) are shown in Fig. 7. These hysteresis loops lead to energy dissipation. It is observed that the hysteretic curves of bearings B1 and B2 are almost the same in two different directions. This means that the superstructure has an approximate ″rigid body″ motion because of the flexible isolation bearings. The friction coefficient μ_1 in this study is set to 0.006, which is a small value, to reduce the structural lateral stiffness in order to prolong the structural periods in the horizontal directions. When the limit displacement in y-direction is reached, the lateral stiffness increases, and the lateral reaction force of the bearing sharply increases to prevent larger horizontal deformation. Fig. 8 shows the motional loci of TFPCs. It is observed that the motional loci of bearings B1 and B2 have only a slight difference. Because there is a horizontal displacement limit, the deformations of bearings are limited to a circular area with a radius of 0.3 m. Clearly, the horizontal sliding displacements of the bearings can be well controlled in the TFPCs.

Fig. 9 shows the hysteretic behaviors of the VDCs in bearings B1 and B2. The energy dissipation values of the VDCs are nearly identical, which are approximately equal to 3500 $N*m$ according to Eq. (3). The damping parameter ξ_v is as high as 265%. The reason that this value is far greater than that of the VDC in *Section 2.3.3* is that the great reduction in stiffness values of K_0 and K_1 leads to a significant reduction in strain energy, and the damping index is inversely proportional to the strain energy parameter according to Eq. (3).

Usually, viscous dampers are typically installed inside structures to increase the structural damping and energy dissipation capacity. However, in this study, the VDCs are installed at the support positions of the dome because they can provide additional vertical flexibility under dynamic loads and provide

additional energy dissipation.

The dome with the hybrid isolation system, which behaves more flexibly, has smaller dynamic demands than the fixed-base structure primarily because the natural vibration periods of the isolation modes, providing most of the response, are much longer than the vibration periods of the fixed-base structure, avoiding coming into the resonance zone with large spectrum acceleration values.

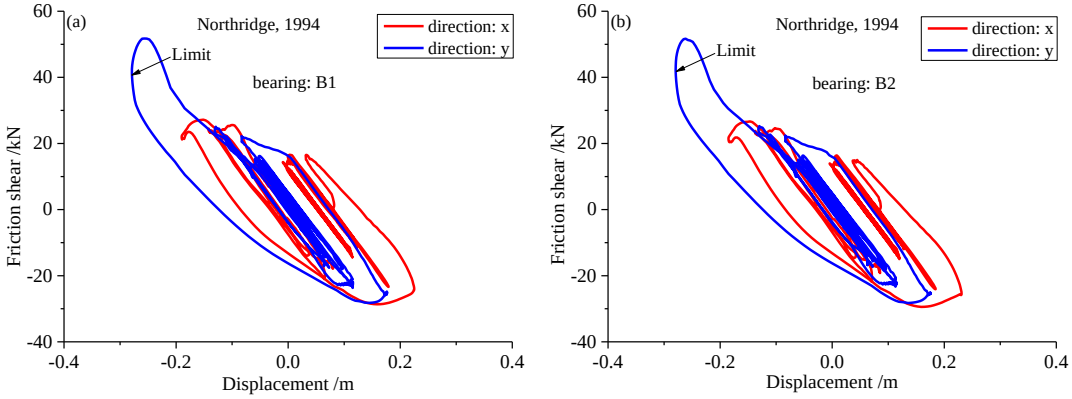

Fig. 7 Hysteretic curves of the TFPCs of bearings (Northridge, 1994).

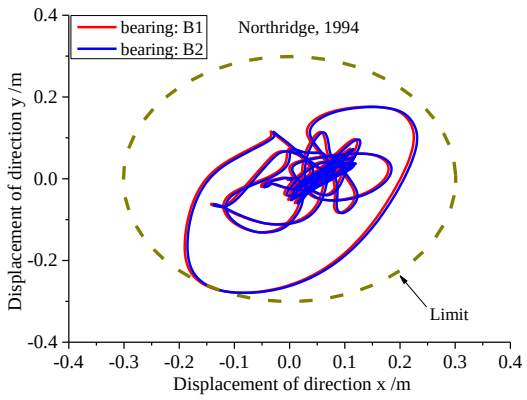

Fig. 8 Motional loci of the TFPCs (Northridge, 1994).

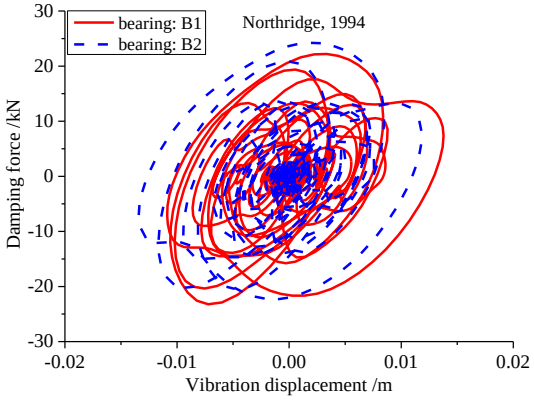

Fig. 9 Hysteretic curves of the VDCs (Northridge, 1994).

4.3 Axial force of typical members

For the dynamic demands of domes, another index that can describe the structural performance is the axial force of a member. The time histories of axial force for member M1 in the O.S and I.S under the Manjil earthquake ground motion are shown in Fig. 10. The axial force of the member is significantly suppressed throughout the earthquake. The vibrating amplitude of the axial force is 1008 kN in the O.S; however, the force is only 201 kN in the I.S, and it decreases by 80%. A significant reduction in the axial force of the member is observed.

The vibrating amplitudes of the axial force for typical members M1 to M6 under 7 near-field ground motions and the isolation effect indexes are listed in Table 9. It is observed that the isolation effect indexes for axial force are within the range of 0.3–0.9; generally, the hybrid isolation system has an excellent isolation effect in axial force; however, for a single earthquake, the isolation effect is not always the same for each member, and the discreteness of the indexes is large.

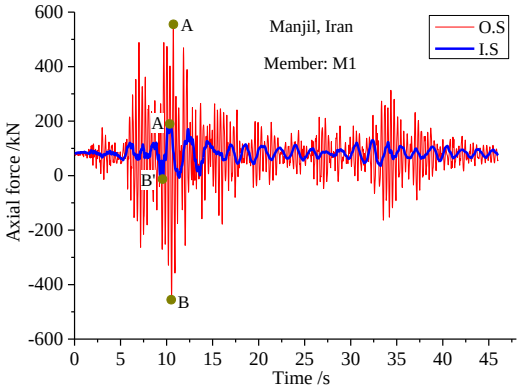

Fig. 10 Time histories of axial force of the member M1 (Manjil, Iran).

Table 9 Vibration amplitudes of the axial force of the O.S and I.S and isolation effect indexes.

Earthquake	Vibration amplitude /kN																	
	M1			M2			M3			M4			M5			M6		
	O.S	I.S	D_f	O.S	I.S	D_f	O.S	I.S	D_f	O.S	I.S	D_f	O.S	I.S	D_f	O.S	I.S	D_f
Imperial Valley	138	80	***0.42***	168	103	***0.39***	128	81	***0.37***	111	62	***0.44***	201	138	***0.31***	156	105	***0.33***
Kobe	790	187	***0.76***	321	198	***0.38***	536	152	***0.72***	609	120	***0.80***	1242	227	***0.82***	443	184	***0.58***
Loma Prieta	923	134	***0.85***	689	173	***0.75***	817	141	***0.82***	1009	128	***0.87***	1497	211	***0.86***	717	162	***0.77***
Chi-Chi	656	258	***0.61***	251	161	***0.36***	428	222	***0.48***	242	125	***0.48***	721	202	***0.72***	243	156	***0.36***
Friuli	805	117	***0.85***	329	162	***0.51***	469	121	***0.74***	416	108	***0.74***	583	188	***0.68***	245	158	***0.36***
Northridge	848	281	***0.67***	333	185	***0.44***	509	196	***0.61***	452	121	***0.73***	871	208	***0.76***	319	172	***0.46***
Manjil	1008	201	***0.80***	401	203	***0.49***	584	173	***0.70***	631	135	***0.79***	1157	254	***0.78***	471	204	***0.57***

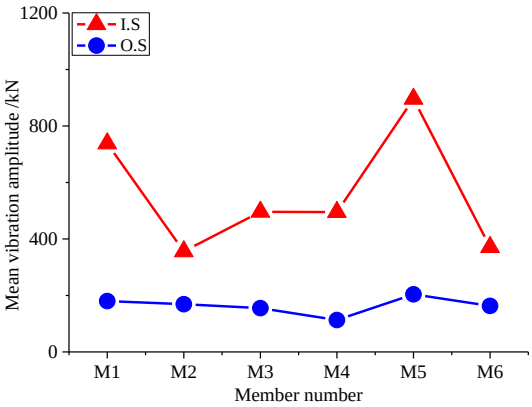

Fig. 11 Mean vibration amplitude of axial force.

The following parameter is defined to compare the differences between the O.S and I.S,

$$\bar{\Delta}_f = \sum_{i=1}^{n} \Delta_{f,i} / n \tag{5}$$

where $\bar{\Delta}_f$ represents the mean amplitude of the axial force of the selected members; $\Delta_{f,i}$ represents the amplitude of the axial force under the i^{th} ground motion; and n is the number of ground motions ($n = 7$). According to Eq. (5), the mean amplitudes of 6 typical members are shown in Fig. 11. They are efficiently reduced. For members M1 and M5, the amplitudes even decrease by approximately 75%–80%, and the hybrid bearings present a better seismic isolation effect for members with high axial force values. Generally, the mean values of the isolation effect indexes in axial force reach approximately 0.4–0.8. This can result in the yielding of fewer members in the isolated structure. The

reduction of the axial force in members can also improve the local stability to avoid the instability of the whole structure. This significantly improves the structural seismic performance. Therefore, the hybrid isolation bearings present superior isolation performance for the dome.

5. Evaluation of seismic isolation effect for the hybrid isolation system

In this section, a more comprehensive index is used to evaluate the seismic isolation effect for the whole structure. The following parameter is defined as the deformation level Δ of the structure by using the displacement amplitudes:

$$\Delta = \sqrt{\frac{\sum_{i=1}^{n} {\Delta_i}^2}{n}} \tag{6}$$

where n is the number of nodes, Δ_i represents the vibration amplitude of the dynamic displacement of i^{th} node in the x, y, or z direction. Here, 17 nodes (from P1 to P17) in the dome are selected to evaluate the structural dynamic deformation levels. According to Eq. (6), the deformation levels of the whole structure under 7 natural near-field ground motions are listed in Table 10. Clearly, the deformations are greatly suppressed due to the use of the proposed hybrid isolation bearings. The mean values of the isolation effect indexes are as high as 0.81, 0.78, and 0.83 in the x, y, and z directions, respectively, except that the mean values are only 0.5–0.7 under Chi-Chi earthquake ground motion. For a given earthquake ground motion, there is only a small difference in the seismic isolation effect for three directions. Generally, the hybrid isolation system has good isolation performance in displacement for the whole structure.

Table 10 Deformation levels of the whole structure and isolation effect indexes.

	Displacement								
Earthquake	*x* /m			*y* /m			*z* /m		
	O.S	I.S	D_f	O.S	I.S	D_f	O.S	I.S	D_f
Imperial Valley	0.0045	6.23e-4	***0.86***	0.006	8.028e-4	***0.86***	0.0072	7.22e-4	***0.90***
Kobe	0.1113	0.0125	***0.88***	0.0733	0.012	***0.84***	0.12	0.015	***0.88***
Loma Prieta	0.08	0.012	***0.85***	0.057	0.008	***0.86***	0.1288	0.018	***0.86***
Chi-Chi	0.0232	0.011	***0.53***	0.0454	0.015	***0.67***	0.0338	0.0122	***0.64***
Friuli	0.0336	0.0089	***0.74***	0.0347	0.0057	***0.84***	0.0582	0.011	***0.81***
Northridge	0.0549	0.0128	***0.77***	0.0452	0.0134	***0.70***	0.0796	0.0159	***0.80***
Manjil	0.0518	0.009	***0.83***	0.0374	0.0104	***0.72***	0.0894	0.015	***0.83***
Mean	**0.0513**	**0.0095**	**0.81**	**0.0427**	**0.0093**	**0.78**	**0.0739**	**0.0125**	**0.83**

6. A comparative study

In this paper, the effectiveness of the proposed isolation bearing has been verified by a large-scale single-layer lattice dome subjected to a limited number of ground motions. Further studies are also needed when applying the proposed hybrid isolation bearing system to engineering practice, especially for the design parameters of the hybrid isolation bearing system and the understanding for the reasons why isolation bearing is effective in reducing dynamic demands for some ground motions and may be ineffective for others, which are discussed in the following sections.

6.1 A comparison in isolation effect between hybrid isolation bearing and the elastic three–spring bearing model

In this study, the parameters of the hybrid isolation bearing system are designed to ensure that the periods of the dominant modes are greater than 1.0 s according to the acceleration spectra. This is realized by shifting the stiffness values of the structural system in three directions. The question,

however, is whether the dynamic demands of the dome can be reduced as long as the flexible bearings are used without considering the energy dissipation capacity of the bearings. For this purpose, the seismic isolation effect of the elastic three–spring bearing (ETSB) model with a lateral limit displacement of 0.3 m is compared with that of the hybrid isolation bearing system in this paper. Here, the dome with the ETSBs is denoted as ″I.Sts″. To make the initial stiffness values of the two structures equal, the stiffness values of the ETSB in the I.Sts are set to 4.28e5 N/m in the horizontal directions and 2.56e5 N/m in the vertical direction. The natural vibration periods of the two structures are listed in Table 11. It can be seen that the two periods are almost the same for each mode, which means that the dynamic characteristics of the two structures are the same. Based on the above 7 natural near-field ground motions, the overall deformations of the structures are evaluated according to Eq. (6) and shown in Fig. 12.

Table 11 Periods of two cases.

	Mode	Mode 1	Mode 2	Mode 3	Mode 4	Mode 5
Period /s	I.S	1.52	1.205	1.205	0.38	0.38
	I.Sts	1.52	1.204	1.204	0.38	0.38
	Mode	Mode 6	Mode 7	Mode 8	Mode 9	Mode 10
Period /s	I.S	0.375	0.375	0.371	0.371	0.37
	I.Sts	0.375	0.375	0.371	0.371	0.37

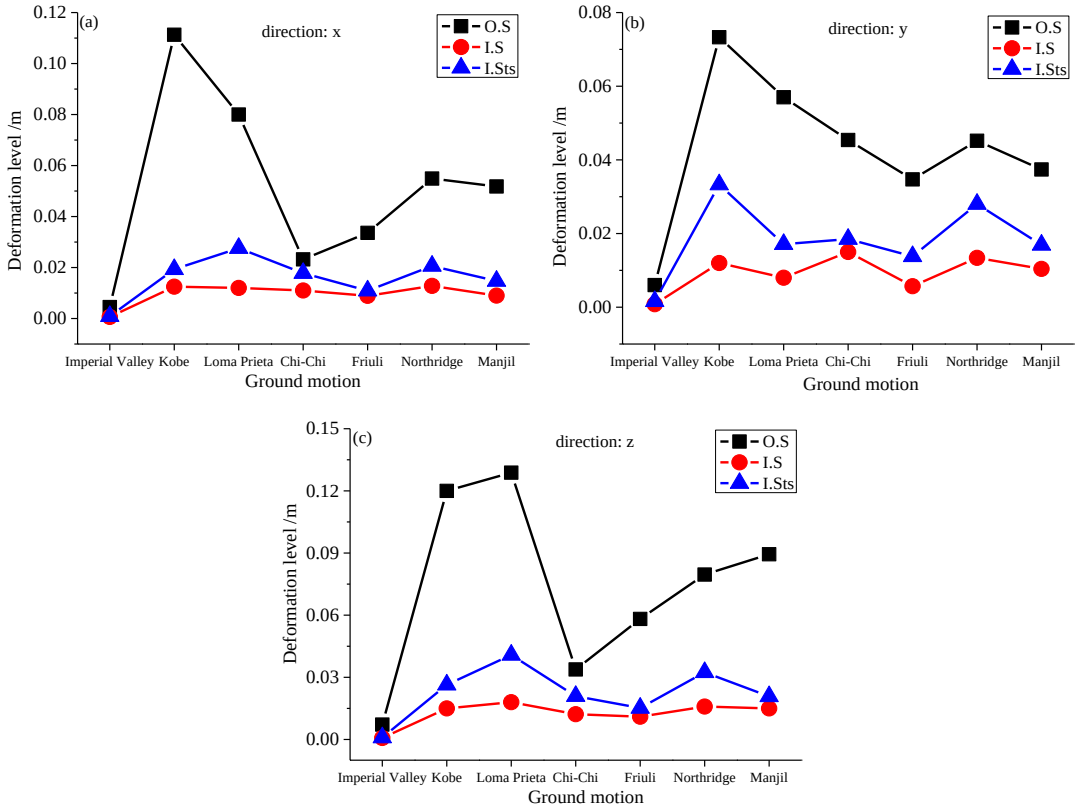

Fig. 12 Difference of displacements in the O.S, I.S, and I.Sts.

Fig. 12 shows that the use of the ETSBs can also significantly suppress the dynamic deformations in all three directions. This is because the flexibility of these bearings prolongs the structural periods, making them correspond to smaller spectrum acceleration values. However, the hybrid isolation bearing has a better seismic isolation effect than the ETSB model; clearly, compared with the ETSB model, this difference is mainly caused by the additional energy dissipation in the hybrid isolation

bearing. The added damping in the hybrid bearing allows part of the earthquake energy to be absorbed, and it reduces the displacement amplitudes to some extent. Therefore, the primary reason for the effectiveness of bearing isolation in reducing earthquake-induced dynamic demands is the prolonging of the dominant-mode periods, while the added damping in the isolation system and associated energy dissipation may only be a secondary factor in reducing dynamic demands. In addition, whether the dynamic demands in the structure are reduced also depends on the spectrum shape and other factors.

6.2 Vertical stiffness of the hybrid isolation bearing

The vertical stiffness in the hybrid isolation bearing has a significant effect on the structural periods in the vertical direction. A reasonable design for this vertical stiffness parameter can shift the structural periods to effectively avoid large spectrum acceleration values. In the proposed hybrid isolation system, the vertical stiffness can be adjusted flexibly by changing the spring stiffness K_1. However, not all the stiffness values can make the hybrid isolation bearing system effective in reducing dynamic demands. Here, three different vertical stiffness values that are set to 5e6 N/m (Stiffness 1), 1e7 N/m (Stiffness 2), and 5e7 N/m (Stiffness 3) are compared in seismic isolation effect. The Northridge ground motion is used for the dynamic analysis. The displacement amplitudes at the top and the amplitudes of axial forces for members M1, M3, and M5 are shown in Fig. 13.

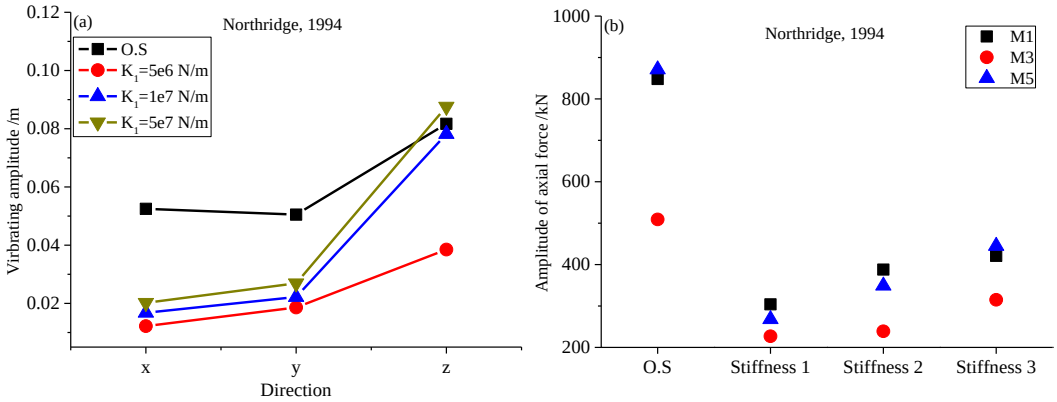

Fig. 13 Effect of the structural vertical stiffness on the isolation effect.

Fig. 13 shows that the ETSBs with the above different stiffness values have a good seismic isolation effect in horizontal displacements, but the displacement amplitudes increase as the stiffness increases, and the seismic isolation performance becomes poor, especially for the stiffness value $K_1 = 5e7\ N/m$, its use in the dome may be detrimental because the displacement at the top is larger than that of the O.S. In axial force, it can be seen that although the ETSBs with these stiffness values also have a good seismic isolation effect, it becomes poor as the stiffness increases, because a large vertical stiffness reduces the periods and increases the spectrum acceleration values. For this reason, base isolation is rarely used for structure systems with natural periods well into the region with large spectrum acceleration values.

6.3 Horizontal stiffness of the hybrid isolation bearing

In the hybrid isolation bearing, the horizontal stiffness can be controlled by the geometrical parameter R_1 and the stick-slip behaviors in the bearing. Compared with the geometrical parameter, the effect of the friction coefficient on the horizontal stiffness is more direct. The smaller friction coefficient can result in longer periods in horizontal directions. In the bearing, the friction coefficient μ_1 in the inner pendulum is low so that sliding occurs under small earthquakes, while the friction coefficients μ_2 and μ_3 are high enough that sliding occurs during moderate and large earthquakes. Therefore, the initial structural horizontal stiffness depends on the friction coefficient μ_1. In this paper,

the friction coefficients μ_1=0.01 (Coefficient 1), 0.02 (Coefficient 2), and 0.03 (Coefficient 3) are considered to discuss the effect of the friction coefficient on the isolation effect. Here, the Kobe earthquake ground motion is used for the dynamic analysis. The displacement amplitudes at the top and the amplitudes of axial forces of members M1, M3, and M5 under different friction coefficients are shown in Fig. 14.

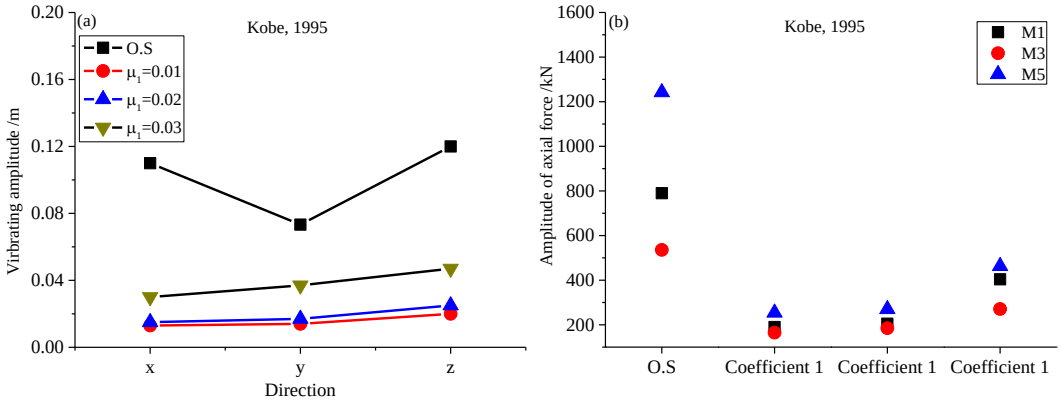

Fig. 14 Effect of the structural horizontal stiffness on the isolation effect.

Fig. 14 shows that all the bearings with these friction coefficients can suppress the dynamic demands of the dome. However, the seismic isolation effect reduces as the friction coefficient increases. Therefore, when using the hybrid bearings, their geometrical and mechanical parameters should be designed carefully according to the acceleration spectra and spectrum shapes. In addition, the horizontal displacements of the bearing should also be considered to avoid large lateral deformations of the structure.

7. Conclusions

In this paper, a hybrid isolation bearing combining a viscous damper component with a triple friction pendulum component and its numerical modeling method are proposed. They are applied to the investigation of a large-scale single-layer lattice dome subjected to earthquake ground motions for three–dimensional seismic isolation purposes. Based on 7 natural near-field ground motions, the good seismic isolation effect for the dome with the hybrid isolation bearings is observed in all three directions. The hybrid isolation bearings can significantly suppress the dynamic displacements of the structure and axial forces of members. For the hybrid bearings, the values of the isolation effect indexes can reach approximately 0.8 in displacement and approximately 0.4–0.8 in axial force, and they present superior performance for seismic isolation. A comparative study shows that the main reason that the base isolation can reduce the structural dynamic demands is the prolonging of the modal periods of the structure, and the damping energy dissipation of the seismic isolation bearings may only be a secondary factor in reducing structural dynamic demands. In the aspect of prolonging the structural periods, two mechanical parameters in this hybrid bearing are discussed for the design purposes in this paper.

Acknowledgements

The authors gratefully acknowledge the financial support provided by the National Key Research and Development Program of China (Grant No. 2018YFC1504304), the Key Project of the Natural Science Foundation of Tianjin, China (Grant No. 19JCZDJC39300) and the National Natural Science Foundation of China (Grant No. 51878433).

References

[1] Jangid RS. Optimum lead-rubber isolation bearings for near-fault motions. Engineering Structures 2007; 29: 2503–2513.

[2] Soong TT, Spencer BF. Supplemental energy dissipation: state-of-the-art and state-of-the-practice. Eng Struct. 2002; 24: 243–259.

[3] Ivanoska-Dacikj A, Bogoeva-Gaceva G, Jurk R, Wiessner S, et al. Assessment of the dynamic behavior of a new generation of complex natural rubber-based systems intended for seismic base isolation. Journal of Elastomers and Plastics 2017; 49(7): 595–608.

[4] Islam ABMS, Al-Kutti WA. Seismic response variation of multistory base-isolated buildings applying lead rubber bearings. Computers and Concrete 2018; 21(5): 495–504.

[5] Zhang HD, Han QH, Wang YF, Lu Y. Explicit modeling of damping of a single-layer latticed dome with an isolation system subjected to earthquake ground motions. Engineering Structures 2016; 106; 154–165.

[6] Wang BF, Han Q, Jia JF. Seismic response analysis of isolated offshore bridge with friction sliding bearings. Earthquakes and Structures 2019; 16(6): 641–654.

[7] Harvey PS, Zehil GP, Gavin HP. Experimental validation of a simplified model for rolling isolation systems. Earthquake Engineering & Structural Dynamics 2014; 43(7): 1067–1088.

[8] Karayel V, Yuksel E, Gokce T, Sahin F. Spring tube braces for seismic isolation of buildings. Earthquake Engineering and Engineering Vibration 2017; 16(1): 219–231.

[9] Nikoomanesh MR, Moeini M, Goudarzi MA. An innovative isolation system for improving the seismic behaviour of liquid storage tanks. International Journal of Pressure Vessels and Piping 2019; 173: 1–10.

[10] Saadatnia M, Riahi HT, Izadinia M. Hysteretic behavior of rubber bearing with yield shear devices. International Journal of Steel Structures 2019, 19(3): 747–759.

[11] Castaldo P , Palazzo B, Alfano G, Palumbo MF. Seismic reliability-based ductility demand for hardening and softening structures isolated by friction pendulum bearings. Structural Control & Health Monitoring 2018, 25(11): 1–27.

[12] Jangid RS. Optimum friction pendulum system for near-fault motions. Engineering Structures 2005, 27: 349 –359.

[13] Constantinou MC, Kalpakidis IV, Filiatrault A, Ecker Lay AE. LRFD-based analysis and design procedures for bridge bearings and seismic isolators. Technical report MCEER-11-0004, Multidisciplinary Center for Earthquake Engineering Research, University at Buffalo, Buffalo, NY, 2011.

[14] Meng QL, Lin DQ, Zhang MZ. Study on three-dimensional isolated system in shaking table test. Earthq Eng Engineering Vib 2007, 27(3):116–120. DOI: 10.1016/S1872-5791(07)60044-X. (in Chinese)

[15] Kikuchi M, Nakamura T, Aiken ID. Three-dimensional analysis for square seismic isolation bearings under large shear deformations and high axial loads. Earthquake Engineering & Structural Dynamics 2010, 39(13): 1513–1531.

[16] Liu WG, Tian K, Wei LS, He WF, Yang QR. Earthquake response and isolation effect analysis. Bulletin of Earthquake Engineering 2018, doi: 10.1007/s10518-018-0417-6.

[17] Takahashi O, Aida H, Suhara J, Matsumoto R, Tsuyuki Y, Fujita T. Construction of civil building using three dimensional seismic isolation system: part 1, design of building using three dimensional seismic isolation system, in: Proceedings, 14th World Conference on Earthquake Engineering, Beijing, China, 2008.

[18] Ryan KL, Soroushian S, Maragakis EM et al (2015) Seismic simulation of an integrated ceiling-partition wall-piping system at E-Defense. I: three-dimensional structural response and base isolation. J Struct Eng 2015, 142(2):04015130.

[19] Lee D, Constantinou MC. Combined horizontal–vertical seismic isolation system for high-voltage-power transformers: development, testing and validation. Bull Earthq Eng 2018:1–24.

[20] Shimada T, Fujiwaka T, Moro S. Study on three-dimensional seismic isolation system for next-generation nuclear power plant: hydraulic three-dimensional base isolation system. In: ASME/JSME 2004 pressure vessels and piping conference. American Society of Mechanical Engineers 2004, 35–42.

[21] Cesmeci S, Gordaninejad F, Ryan KL, Eltahawy W. A liquid spring-magnetorheological damper system under combined axial and shear loading for three-dimensional seismic isolation of structures. Journal of Intelligent of Material Systems and Structures 2018, 29(18): 3517–3532.

[22] Xue SD, Zhuang P, Li BS. Seismic Isolation of Lattice Shells using a New Type of SMA-Rubber Bearings. Proceedings of IASS Symposium 2005, 353–358.

[23] Kim YC, Xue, SD , Zhuang P, Zhao W, Li CH. Seismic isolation analysis of FPS bearings in spatial lattice shell structures. Earthq Eng Engineering Vib 2010, 9(1):93–102.
[24] Zhai Y, Fu X, Chen Y, Hu W. Study on column-top seismic isolation of single-layer latticed domes. Sustainability 2019, 11(3): 1–9. Doi:10.3390/su11030936.
[25] Kong DW, Wang LL, Fan F, Zhi XD. Seismic performance of column supporting single-layer reticulated domes with friction pendulum bearings. International Journal of Steel Structures 2017, 17(2): 471–480.
[26] Kong DW, Wang LL, Wu L, Zhang, YX. Influence of Column Supports on Seismic Performance of K8 Single-Layer Spherical Reticulated Domes with Friction Pendulum Bearings. International Journal of Steel Structures 2019, 19(3): 747–759.
[27] Chen ZT, Ding Y, Shi YD, Li ZX. A vertical isolation device with variable stiffness for long-span spatial structures. Soil Dynamics and Earthquake Engineering 2019, 123: 543-558.
[28] Chen ZT, Ding Y, Shi YD, Li ZX. Research on isolation performance of three-dimensional isolation device with vertical variable stiffness for long-span spatial structures. China Journal of Building Structures 2019, 40(10): 35–42. DOI: 10.14006/j.jzjgxb.2019.0019. (in Chinese)
[29] Li XY, Xue SD, Cai YC. Three-dimensional seismic isolation bearing and its application in long span hangars. Earthq Eng & Eng Vib 2013, 12: 55–65.
[30] Park SW, Ghasemi H, Shen J. Simulation of the seismic performance of the Bolu viaduct subjected to near-fault ground motions. Earthquake Engineering and Structural Dynamics 2004, 33(4): 1249–1270.
[31] Dao ND, Ryan KL, Sato E, Sasaki T. Predicting the displacement of triple pendulum™ bearings in a full-scale shaking experiment using a three-dimensional element. Earthquake Engineering and Structural Dynamics 2013; 42: 1677–1695.
[32] Fenz DM, Constantinou MC. Spherical sliding isolation bearings with adaptive behavior: Theory. Earthquake Engineering and Structural Dynamics 2008; 37(2):163–183.
[33] Bowden F.P., Tabor D. The friction and lubrication of solids – part II. Oxford University Press, London, Great Britain, 1964.
[34] Constantinou MC, Mokha A, Reinhorn A. Teflon bearings in base isolation. II: Modeling. Journal of Structural Engineering (ASCE) 1990; 116(2): 455–474.
[35] Mokha A, Constantinou MC, Reinhorn AM, Zayas VA. Experimental study of friction–pendulum isolation system. Journal of Structural Engineering 1991; 117(4): 1201–1207.
[36] Akcelyan S, Lignos DG, Hikino T. Adaptive numerical method algorithms for nonlinear viscous and bilinear oil damper models subjected to dynamic loading. Soil Dynamics and Earthquake Engineering 2018, 113:488–502.
[37] Computers and Structures, Inc. (CSI). CSI Perform-3D User Guide. Berkeley, California, USA, 1995.
[38] Hall JF. Problems encountered from the use (or misuse) of Rayleigh damping. Earthquake Engineering & Structural Dynamics 2006; 35(5): 525–545.